LAWRENCE
LIVERMORE
NATIONAL
LABORATORY

UCRL-JRNL-200561

Performance of a phase-conjugate-engine implementing a finite-bit phase correction

K.L. Baker, E.A. Stappaerts, S.C. Wilks, P.E. Young, D.T. Gavel, J.W. Tucker, D.A. Silva, S.S. Olivier

October 24, 2003

Optic Letters

DISCLAIMER

This work was performed under the auspices of the U. S. Department of Energy by the University of California, Lawrence Livermore National Laboratory under Contract No. W-7405-Eng-48.

Performance of a phase-conjugate-engine implementing a finite-bit phase correction

K.L. Baker, E.A. Stappaerts, S.C. Wilks, D. Gavel, P.E. Young, J. Tucker, S.S. Olivier, D.A. Silva and J. Olsen

Lawrence Livermore National Laboratory, Livermore, CA, USA

Abstract

This article examines the achievable Strehl ratio when a finite-bit correction to an aberrated wave-front is implemented. The phase-conjugate-engine (PCE) used to measure the aberrated wave-front consists of a quadrature interferometric wave-front sensor, a liquid-crystal spatial-light-modulator and computer hardware/software to calculate and apply the correction. A finite-bit approximation to the conjugate phase is calculated and applied to the spatial light modulator to remove the aberrations from the optical beam. The experimentally determined Strehl ratio of the corrected beam is compared with analytical expressions for the expected Strehl ratio and shown to be in good agreement with those predictions.

OCIS codes: 010.1080, 010.7350, 120.2880, 090.1000

This article examines the mean square error arising from the use of a finite-bit correction to an aberrated wave-front. In the context of this article, the finite-bit number of phase correction levels refers to a binary correction scheme with each increase in bits representing a factor of two in correction levels. A one-bit phase correction represents two phase correction levels, 2^1, and a two-bit phase correction represents four phase correction levels, 2^2, etc. A finite-bit correction or discretized correction can be applied for various reasons. Bistable spatial light modulators such as ferroelectric liquid-crystal spatial light modulators, for instance, are potentially suitable for binary wave-front correction levels or one-bit operation.[1] Nematic liquid-crystal spatial light modulators typically accept eight-bit input signals, however, their nonlinear response curves generally limit their response to ~six bits, 2^6 phase levels. MEMS-based spatial light modulators are becoming more prevalent and are beginning to transition to devices with on-chip electronics. The electronics for these mirrors can be designed to receive either analog or digital, discretized, voltages to control the mirror's deflection. In the case of discretized voltages, the performance of these mirrors will vary according to their displacement vs. voltage response curves and to the number of bits in their A/D convertors, both of which will determine the number of phase levels in the correction. A finite-bit number of corrections, for numbers ≤ 3, can be very efficiently implemented in software in the case of interferometric wave-front sensors as discussed below. It can also be used to increase the field-of-view of the adaptive optical system by going to a smaller number of phase levels for the correction.[2]

In this article, an experimental study is conducted to examine the effects of a finite-bit correction to the achievable Strehl ratio of the system under conditions of a high scintillation index. The phase conjugate engine (PCE) used to measure the aberrated wave-front consists of a quadrature interferometric wave-front sensor, a liquid crystal spatial light modulator (LC-SLM) and computer hardware/software to calculate and apply the correction. The wave-front sensor measures the phase associated with the aberrated beam. The conjugate phase is calculated and a discretized version of

the phase is applied to the LC-SLM to remove the aberrations from the optical beam. For a one bit correction to the wave-front error, the phase correction is discretized to two levels, $\pi/2$ and $3\pi/2$, that lie in the middle of the two phase ranges 0 and π and between π and 2π radians, respectively. This would then represent a binary adaptive optic.[1] Control of two bits allows four phase correction points placed between 0 to $\pi/2$, $\pi/2$ to π, π to $3\pi/2$ and $3\pi/2$ to 2π degrees, etc.

The optical layout of the AO system is shown in Figure 1. It consists primarily of an interferometric wave-front sensor, a Hamamatsu parallel-aligned nematic liquid-crystal spatial-light-modulator (LC-SLM)[3-5] and computer hardware/software to analyze and implement the phase correction. The probe laser is a 532 nm frequency-doubled Nd:YAG microchip laser with a pulse energy of 1 μJ and a repetition rate of over 5 khz. The vertically polarized laser output is split into two separate beams, a reference beam and a probe beam. The probe beam passes through three aberrating phase plates that were designed to simulate atmospheric turbulence with a Kolmogorov phase structure function.[5] After traversing the phase plates, the probe beam passes though an aperture that is relay imaged onto the LC-SLM. It is then reflected from the LC-SLM and recombined with the reference beam after being reflected by two 50/50 beamsplitters. The reference beam passes through a quarter wave plate (QWP), which converts the linearly polarized light into circularly polarized light with the orthogonal polarizations 90 degrees out of phase with one another. After passing through the QWP, the reference and probe beams are combined using a non-polarizing 50/50 beamsplitter. Both beams then pass through a half wave plate that rotates their polarization by $\pi/4$, producing equal amplitude horizontal and vertical components of the probe beam while maintaining the $\pi/2$ phase shift between the horizontal and vertical components of the reference beam. The beams then pass through a telescope, which images the LC-SLM onto the charge-coupled device (CCD) array. A Wollaston prism, at the focus of the first telescope lens, separates the two interferograms in angle. The two interferograms, having orthogonal polarizations, exit the Wollaston

prism at an angle of approximately 1.65 degrees with respect to one another and are collimated by the lens placed directly after the Wollaston prism. The two spatially separated interferograms are then directed to the CCD camera, which is in a conjugate plane to the spatial light modulator and to the entrance aperture of the system. Upon determining the aberrated phase of the probe beam, the conjugate phase is applied to the LC-SLM and a separate HeNe laser operating at 543 nm, labeled the comm. laser in Fig. 1, is reflected off of the spatial light modulator. The LC-SLM applies a pre-correction to the HeNe laser beam before it back propagates through the atmospheric phase plates and the point-spread function is measured with a far-field diagnostic.

This interferometric approach to wave-front sensing provides a straightforward approach to increase the speed of the phase determination procedure. One of the interferograms measures the sine of the phase and the other the cosine of the phase. By directly comparing the intensity between the two interferograms, the phase can be determined with a finite-bit resolution. The flowchart of the algorithm used to determine the phase is shown in Figure 2. In the case of a one bit correction, if the intensity of the sine channel is greater than zero then the phase measured lies between 0 and π and if the sine channel is less than zero then the phase measured lies between $-\pi$ and 0. The inverse phase applied to the LC-SLM would be $3\pi/2$ for the phase measured between 0 and π and $\pi/2$ for the phase measured between $-\pi$ and 0. Fig. 2 also indicates the algorithm used for the two bit and three bit corrections as labeled. To break the measured phase into quadrants, it becomes necessary to know both whether the sine intensity is positive or negative, as well as, whether the cosine intensity is positive or negative. The three-bit correction then also requires the knowledge of whether the sine intensity is greater or less than the cosine intensity. As shown below the maximum Strehl ratio achievable with a three-bit correction is approximately 95% signifying that there are diminishing returns for the added complexity of going beyond a three-bit correction.

Figure 3 shows a representative uncorrected far-field image and near-field image taken with the adaptive optics system shown in Figure 1. The near-field image is highly scintillated with a scintillation index of 1.2. The uncorrected far-field image shows that the beam is highly aberrated after passing through three phase screens with a Kolmogorov turbulence spectrum. After measuring the aberrated phase and following the algorithm outlined in Fig. 2, the conjugate phase is applied to the LC-SLM. The resultant corrected far-field images for four different finite-bit corrections applied to the liquid crystal spatial light modulator are then shown in Fig. 4. The correction bits range from one-bit correction in Fig. 4a to an approximate six-bit correction in Fig. 4d. The six-bit correction was obtained by taking the arctangent of the cosine and sine channels and accounting for the nonlinear response of the LC-SLM. There is a steady increase in intensity as the bit approximation is improved with the largest increase occurring between the one-bit and two-bit corrections. The relative Strehl ratio, measured from the point-spread functions displayed in Fig. 4, are displayed in Fig. 5 as the solid gray squares representing the one-bit, two-bit, three-bit and six-bit corrections. The results are plotted against analytical estimates detailed below.

In the "spirit" of adaptive optics, the mean square phase error, or phase variance, for a finite-bit approximation can be calculated and the Strehl ratio approximated using the Marechal approximation, $S_r \sim EXP(-\sigma^2)$. For a given number of bits, n, the number of phase correction levels is given by 2^n. Each level of correction covers a phase region of $\phi_o = 2\pi/2^n$ radians. The variance of the phase, σ^2, within each of the correction levels can be expressed by the sum

$$\sigma^2 = \frac{1}{m}\sum_{i=0}^{m-1}\left(\phi_i - \phi_{avg}\right)^2, \qquad (1)$$

where m represents the number of phases within the correction level and ϕ_{avg} is the central phase within a particular correction level. Assuming the distribution of phases within a given correction interval is uniform, the sum in Eq. 1 can be expressed as the integral

$$\sigma^2 \approx \frac{1}{\phi_o}\int_0^{\phi_o}(\phi-\phi_o/2)^2\,d\phi = \left(\frac{\pi^2}{3}\right)\frac{1}{2^{2n}}. \qquad (2)$$

Using the "extended Marechal approximation", the Strehl ratio, S_r, can be expressed as the $S_r \sim EXP\{-(\pi^2/3)/2^{2n}\}$. Figure 2 shows a comparison between the Strehl ratio derived above, and a more formal derivation, which arrived at the expression $S_r = \mathrm{sinc}^2(\pi/2^n)$.[1] In Fig. 2, the more formal derivation is represented by the black circles and the approximate Strehl ratio obtained from Eq. 2 is displayed by the solid gray line. The percentage difference between these two Strehl ratios is then shown as the dashed gray line, which shows a maximum error of 8 percent for the one-bit correction, which quickly falls off to less than 0.5 percent for a two-bit phase correction.

In summary, the performance of an AO system given a finite-bit approximation to the phase correction was measured. As discussed in the introduction, the finite-bit phase correction can be driven by the SLM technology, as in the case of ferroelectric LC-SLM or digital MEMS-based SLMs containing finite-bit A/D convertors, or by system tradeoffs such as speed or field-of-view. The measured Strehl ratio agreed well with analytical estimates of the expected Strehl ratio, which assumed that the phases were randomly distributed.

The authors would like to acknowledge H. Komine for suggesting a Wollaston prism, in the configuration shown in Figure 1, for channel separation on the CCD camera. The authors would also like to thank L. Flath and M. Kartz for assistance on computer software and hardware, respectively. This effort was sponsored by the Defense Advanced Research Projects Agency (DARPA) for work on the Coherent Communications, Imaging and Targeting (CCIT) program, 02-L493. This work was performed under the auspices of the U.S. Department of Energy by the University of California, Lawrence Livermore National Laboratory under contract No. W-7405-Eng-48.

REFERENCES

[1] G. D. Love, N. Andrews, P. Burch, et al., "Binary adaptive optics: atmospheric wave-front correction with a half-wave phase shifter," Applied Optics **34**, 6058 (1995).

[2] E. Stappaerts, K. Baker, D. Gavel, et al., "Coherent Communications, Imaging and Targeting," in *2004 IEEE Aerospace Conference*, edited by IEEE (IEEE, Big Sky, MT, 2004).

[3] K. L. Baker, E. A. Stappaerts, S. C. Wilks, et al., "Open and Closed-Loop Aberration Correction using a Quadrature Interferometric Wave-Front Sensor," Optics Letters (2003).

[4] C. J. Buchenauer and A. R. Jacobson, "Quadrature Interferometer for plasma density measurements," Rev. Sci. Instrum. **48**, 769 (1977).

[5] J. W. Hardy, *Adaptive Optics for Astronomical Telescopes* (Oxford University Press, Oxford, 1998).

FIGURE CAPTIONS

Figure 1 Closed-loop adaptive optics layout: BS, beam splitters; M, mirrors; L, lenses; I, iris; IF, interference filter; $\lambda/2$ and $\lambda/4$, half and quarter wave-plates, respectively.

Figure 2 Algorithm flowchart used to determine the finite-bit phase from the sine and cosine interferograms.

Figure 3 Uncorrected far-field image and near-field image taken with the adaptive optics system shown in Figure 1.

Figure 4 Finite-bit corrected point-spread functions. The one-bit, two-bit, three-bit and six-bit corrected far-field images are displayed in Fig. 4a, Fig. 4b, Fig. 4c and Fig. 4d, respectively.

Figure 5 Strehl ratio values as a function of bit corrections. The analytical Strehl ratio values are represented by the black circles and the solid gray line, with the percentage error between the two expressions displayed as the dashed gray line. The measured Strehl ratio values, using the data displayed in Figure 4, are displayed as the solid gray squares representing the one-bit, two-bit, three-bit and six-bit corrections.

FIGURES

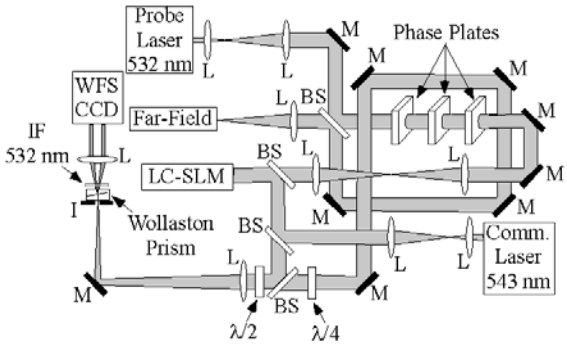

Figure 1

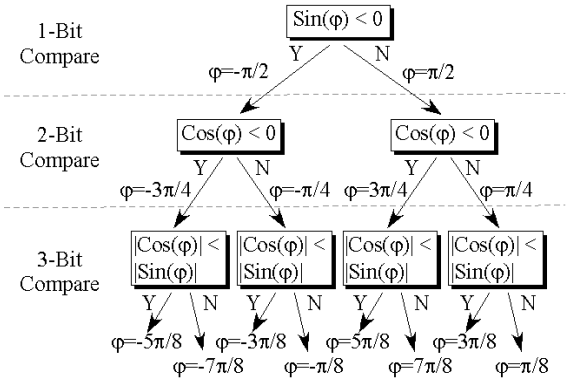
1-Bit Compare
2-Bit Compare
3-Bit Compare
Sin(φ) < 0
Y
N
φ=-π/2
φ=π/2
Cos(φ) < 0
Cos(φ) < 0
φ=-3π/4
φ=-π/4
φ=3π/4
φ=π/4
|Cos(φ)| < |Sin(φ)|
φ=-5π/8
φ=-7π/8
φ=-3π/8
φ=-π/8
φ=5π/8
φ=7π/8
φ=3π/8
φ=π/8

Figure 2

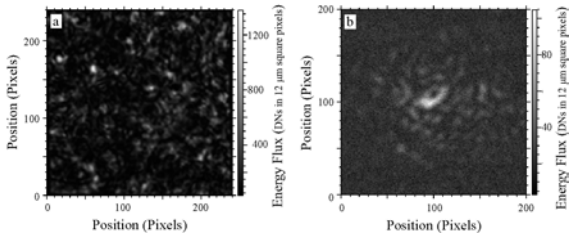
a
b
Position (Pixels)
Energy Flux (DNs in 12 μm square pixels)
0
100
200
400
800
1200
40
80

Figure 3

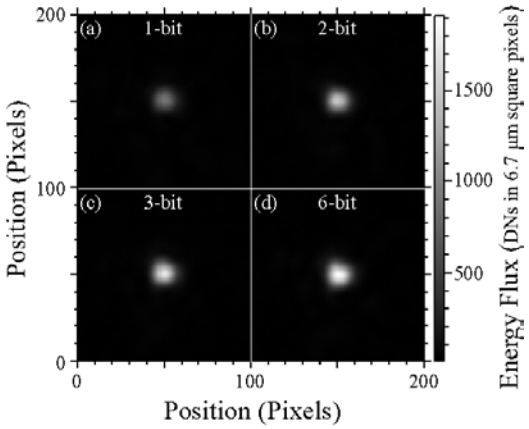
(a) 1-bit
(b) 2-bit
(c) 3-bit
(d) 6-bit
200
100
0
0
100
200
Position (Pixels)
Position (Pixels)
1500
1000
500
Energy Flux (DNs in 6.7 μm square pixels)

Figure 4

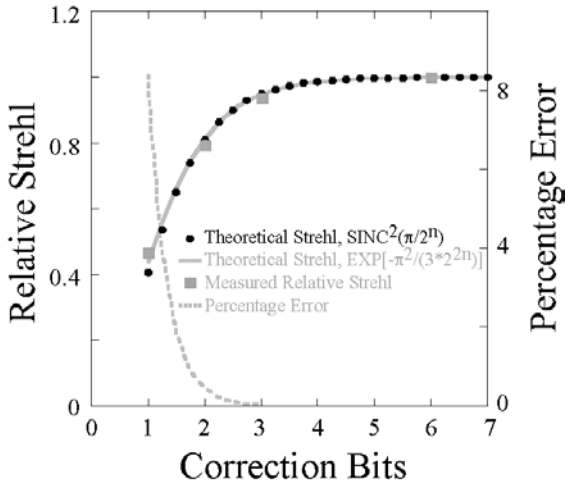
1.2
0.8
0.4
0
0
1
2
3
4
5
6
7
8
4
0
Relative Strehl
Percentage Error
Correction Bits
Theoretical Strehl, SINC2(π/2n)
Theoretical Strehl, EXP[-π2/(3*22n)]
Measured Relative Strehl
Percentage Error

Figure 5

University of California
Lawrence Livermore National Laboratory
Technical Information Department
Livermore, CA 94551